
Continuous Tensor Relaxation for Finding Diverse Solutions in Combinatorial Optimization Problems

Yuma Ichikawa*

Fujitsu Limited, Kanagawa, Japan,
ichikawa.yuma@fujitsu.com
Graduate School of Arts and Sciences,
University of Tokyo, Tokyo, Japan
ichikawa-yuma1@g.ecc.u-tokyo.ac.jp

Hiroaki Iwashita

Fujitsu Limited, Kanagawa, Japan,
iwashita.hiroak@fujitsu.com

Abstract

Finding the best solution is a common objective in combinatorial optimization (CO). In practice, directly handling constraints is often challenging, incorporating them into the objective function as the penalties. However, balancing these penalties to achieve the desired solution is time-consuming. Additionally, formulated objective functions and constraints often only approximate real-world scenarios, where the optimal solution is not necessarily the best solution for the original real-world problem. One solution is to obtain (i) *penalty-diversified solutions* with varying penalty strengths for the former issue and (ii) *variation-diversified solutions* with different characteristics for the latter issue. Users can then post-select the desired solution from these diverse solutions. However, efficiently finding these diverse solutions is more difficult than identifying one. This study introduces Continual Tensor Relaxation Annealing (**CTRA**) for unsupervised-learning (UL)-based CO solvers, a computationally efficient framework for finding these diverse solutions in a single training run. The key idea is to leverage representation learning capability to automatically and efficiently learn common representations and parallelization. Numerical experiments show that CTRA enables UL-based solvers to find these diverse solutions much faster than repeatedly running existing UL-based solvers.

1 Introduction

Constrained combinatorial optimization (CO) problems aim to find the optimal solution within a feasible space, a fundamental problem in various scientific and engineering applications [Papadimitriou and Steiglitz, 1998, Korte et al., 2011]. However, practical scenarios often necessitate a diverse set of solutions rather than a single optimal one, primarily due to following two key situations.

The first situation involves incorporating constraints of a CO problem as penalties into the cost function, transforming it into an unconstrained CO problem. This approach is employed when directly handling hard constraints is challenging or when allowing some degree of constraint violation is permissible to explore solutions with a lower cost function. However, controlling the trade-off between the cost function and the penalties to achieve the desired solutions can be time-consuming. To address this, efficiently searching for a set of solutions with varying penalty strengths—referred to as (i) *penalty-diversified solutions*—is a viable strategy. Once penalty-diversified solutions are obtained, users can select the most suitable solution during post-processing, as illustrated in Fig. 1.

The second situation can be necessary when the formulated cost function or constraints only approximate a complex real-world problem. These simplified formulations often capture only a part of the real-world problem, failing to consider important aspects of modeling and implicit conditions that users may have. In such cases, the optimal solution for the simplified formulation may not always be

desirable in practice. To address this, exploring a set of solutions with diverse characteristics and reasonably good performance—referred to as (ii) *variation-diversified solutions*—is advantageous. These diverse solutions allow users to choose the best solution tailored to real-world complexities during post-processing, as shown in Fig. 1. They not only address modeling limitations but are also beneficial in various applications. For example, in molecular design optimization, obtaining solutions that meet desired properties while exhibiting a variety of variations is beneficial [Pereira et al., 2021]. However, efficiently finding these diverse solutions is more challenging than identifying one.

To tackle these issues, we propose Continual Tensor Relaxation Annealing (**CTRA**) method for unsupervised learning (UL)-based CO solvers [Schuetz et al., 2022a, Karalias and Loukas, 2020], computationally efficient framework for finding diverse solutions in a single training run by effectively using GPUs. CTRA uses the same neural network as the UL-based solver which outputs a single solution, leveraging the learning of common representations across multiple problem instances and enabling efficient and automatic parallelization in representation space. This approach allows for exploring diverse solutions with a comparable number of model parameters and runtime to those of UL-based solvers that produce a single solution. Numerical experiments demonstrate it in three benchmark CO problems. Additionally, CTRA enhances the search capabilities, resulting in higher-quality solutions compared to existing UL-based solvers that output a single solution and greedy algorithms.

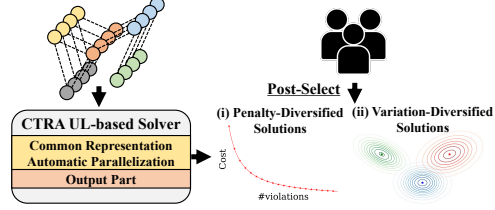


Figure 1: Overview of CTRA UL-based solver and post-processing for diverse solutions.

Notation We use the shorthand expression $[N] = \{1, 2, \dots, N\}$, $N \in \mathbb{N}$. $I_N \in \mathbb{R}^{N \times N}$ represents an identity matrix of size $N \times N$. Here, $\mathbf{1}_N$ denotes the vector $(1, \dots, 1)^\top \in \mathbb{R}^N$, and $\mathbf{0}_N$ denotes the vector $(0, \dots, 0)^\top \in \mathbb{R}^N$. $G(V, E)$ denotes an undirected graph, where V is the set of nodes and $E \subseteq V \times V$ is the set of edges. For a graph $G(V, E)$, A_{ij} denote the adjacency matrix with $A_{ij} = 0$ if an edge (i, j) does not exist and $A_{ij} > 0$ if the edge connects. $\mathbb{V}\text{AR}[\{a_k\}_{k=1}^K]$ represents the empirical variance $\sum_{k=1}^K (a_k - \sum_{k'=1}^K a_{k'}/K)^2 / K$, and $\text{STD}[\{a_k\}_{k=1}^K]$ denotes the empirical standard deviation $(\mathbb{V}\text{AR}[\{a_k\}_{k=1}^K])^{1/2}$. For binary vectors $\mathbf{a}, \mathbf{b} \in \{0, 1\}^N$, we define the Hamming distance as $d_H(\mathbf{a}, \mathbf{b}) = \sum_{i=1}^N \mathbf{1}[a_i \neq b_i]$, where $\mathbf{1}[\cdot]$ denotes the indicator function.

2 Background

Combinatorial optimization The goal of this study is to solve constrained CO problems as follows:

$$\min_{\mathbf{x} \in \mathcal{X}(C)} f(\mathbf{x}; C), \quad \mathcal{X}(C) = \left\{ \mathbf{x} \in \{0, 1\}^N \mid \begin{array}{l} g_i(\mathbf{x}; C) \leq 0, \quad \forall i \in [I], \\ h_j(\mathbf{x}; C) = 0 \quad \forall j \in [J] \end{array} \right\}, \quad (1)$$

where $C \in \mathcal{C}$ denotes instance parameters, such as a graph $G = (V, E)$. $f : \mathcal{X} \times \mathcal{C} \rightarrow \mathbb{R}$ denotes the cost function and $g_i : \mathcal{X} \times \mathcal{C} \rightarrow \mathbb{R}$ and $h_j : \mathcal{X} \times \mathcal{C} \rightarrow \mathbb{R}$ denote constraints. The binary vector $\mathbf{x} = (x_i)_{1 \leq i \leq N} \in \{0, 1\}^N$ is to be optimized, and $\mathcal{X}(C)$ denotes the feasible solution space. In practical scenarios, constrained CO problems are often transformed into unconstrained CO problems using the penalty method:

$$\min_{\mathbf{x} \in \{0, 1\}^N} l(\mathbf{x}; C, \boldsymbol{\lambda}), \quad l(\mathbf{x}; C, \boldsymbol{\lambda}) \triangleq f(\mathbf{x}; C) + \sum_{i=1}^{I+J} \lambda_i v_i(\mathbf{x}; C). \quad (2)$$

Here, for all $i \in [I+J]$, $v_i : \{0, 1\}^N \times \mathcal{C} \rightarrow \mathbb{R}$ is the penalty term that increases when constraints are violated. For instance, the penalty term is defined as follows:

$$\forall i \in [I], v_i(\mathbf{x}; C) = \max(0, g_i(\mathbf{x}; C)), \quad \forall j \in [J], v_j(\mathbf{x}; C) = (h_j(\mathbf{x}; C))^2, \quad (3)$$

and $\boldsymbol{\lambda} = (\lambda_i)_{1 \leq i \leq I+J} \in \mathbb{R}^{I+J}$ represents the penalty parameters that balance satisfying the constraints and optimizing the cost function. Note that the penalty for violations of the constraints becomes more significant as $\boldsymbol{\lambda}$ increases. Tuning these penalty parameters $\boldsymbol{\lambda}$ to achieve the desired solutions is a challenging and time-consuming task. It often necessitates solving the problem repeatedly while adjusting the penalty parameters $\boldsymbol{\lambda}$ until an acceptable solution is found.

Continuous relaxation and UL-based solvers The continuous relaxation strategy reformulate a CO problem by converting discrete variables into continuous ones as follows:

$$\min_{\mathbf{p} \in [0,1]^N} \hat{l}(\mathbf{p}; C, \boldsymbol{\lambda}), \quad \hat{l}(\mathbf{p}; C, \boldsymbol{\lambda}) \triangleq \hat{f}(\mathbf{p}; C) + \sum_{i=1}^{m+p} \lambda_i \hat{v}_i(\mathbf{p}; C),$$

where $\mathbf{p} = (p_i)_{1 \leq i \leq N} \in [0, 1]^N$ represents relaxed continuous variables, i.e., each binary variable $x_i \in \{0, 1\}$ is relaxed to a continuous one $p_i \in [0, 1]$, and $\hat{f} : [0, 1]^N \times \mathcal{C} \rightarrow \mathbb{R}$ is the relaxation of f , satisfying $\hat{f}(\mathbf{x}; C) = f(\mathbf{x}; C)$ for $\mathbf{x} \in \{0, 1\}^N$. The relation between the constraint v_i and its relaxation \hat{v}_i is similar for $i \in [I + J]$, i.e., $\forall i \in [I + J], \hat{v}_i(\mathbf{x}; C) = v_i(\mathbf{x}; C)$ for $\mathbf{x} \in \{0, 1\}^N$.

UL-based solvers employ this continuous relaxation strategy for training neural networks. Wang et al. [2022], Schuetz et al. [2022a], Karalias and Loukas [2020]. Here, the relaxed continuous variables are parameterized by $\boldsymbol{\theta}$ as \mathbf{p}_θ and then optimized by directly minimizing the following loss function:

$$\hat{l}(\boldsymbol{\theta}; C, \boldsymbol{\lambda}) \triangleq \hat{f}(\mathbf{p}_\theta(C); C) + \sum_{i=1}^{I+J} \lambda_i \hat{v}_i(\mathbf{p}_\theta(C); C). \quad (4)$$

After training, the relaxed solution \mathbf{p}_θ is transformed into discrete variables by artificial rounding \mathbf{p}_θ , such that $\forall i \in [N], x_i = \text{int}(p_{\theta,i}(C))$ using a threshold [Schuetz et al., 2022a], or via a greedy method [Wang et al., 2022]. Based on this formulation, two types of schemes have been developed.

(I) Learning generalized heuristics from history/data One approach, proposed by Karalias and Loukas [2020], aims to automatically learn typically effective heuristics from history/dataset instances $\mathcal{D} = \{C_\mu\}_{\mu=1}^P$ and then apply these learned heuristics to new instance C^* through inference. Note that this method assumes that the training dataset can be easily obtained or that meaningful data augmentation is possible. Specifically, given a set of training instances $\mathcal{D} = (C_\mu)$, IID sampled from a distribution $P(C)$, the goal is to minimize the averaged loss function $\min_{\boldsymbol{\theta}} \sum_{\mu=1}^P l(\boldsymbol{\theta}; C_\mu, \boldsymbol{\lambda})$. However, this method cannot guarantee quality for a test instance C^* . Even if the training instances \mathcal{D} are numerous and the test instance C also follows $P(C)$, a low averaged performance $\mathbb{E}_{C \sim P(C)}[\hat{l}(\boldsymbol{\theta}; C)]$ may not ensure a low $l(\boldsymbol{\theta}; C)$ for a specific C . To address this issues, Wang and Li [2023] introduced a meta-learning approach, where NNs aim for good initialization for future instances rather than direct solutions.

(II) Learning effective heuristics on a specific single instance Another approach, referred to as the PI-GNN solver [Schuetz et al., 2022a,b], automatically learns instance-specific heuristics for a given single instance using the instance parameter C by directly employing Eq. (4). This approach studied CO problems on graphs, i.e., $C = G(V, E)$, and employed graph neural networks (GNN) for the relaxed variables $\mathbf{p}_\theta(G)$. Here, an L -layered GNN is trained to directly minimize $\hat{l}(\boldsymbol{\theta}; C, \boldsymbol{\lambda})$ in Eq. (4), taking as input a graph G and the embedding vectors on the nodes, and outputting the relaxed solution $\mathbf{p}_\theta(G) \in [0, 1]^N$. A detailed description of GNNs is given in Appendix B.1. Note that this setting is applicable even when the training dataset \mathcal{D} is not easily obtainable. However, learning to minimize Eq. (4) for a single instance can be time-consuming compared to the inference process. Nonetheless, for large-scale problems, it has demonstrated superiority over other solvers in terms of both time and solution performance [Schuetz et al., 2022a,b].

UL-based solvers face two practical issues: optimization issues, where they are easily trapped in local optima, and rounding issues, where they require artificial post-learning rounding from the continuous space back to the original discrete space, undermining the robustness of the results. To address the former issue, Ichikawa [2023], Sun et al. [2022], Sanokowski et al. [2024] proposed annealing schemes to escape local optima by introducing the following entropy term:

$$\hat{r}(\boldsymbol{\theta}; C, \boldsymbol{\lambda}, \gamma) = \hat{l}(\boldsymbol{\theta}; C, \boldsymbol{\lambda}) + \gamma s(\boldsymbol{\theta}; C), \quad (5)$$

where the entropy term has two different forms:

$$s(\boldsymbol{\theta}; C) = \begin{cases} \sum_{i=1}^N \{(2p_{\theta,i}(C) - 1)^\alpha - 1\}, & \alpha \in \{2n - 1 \mid n \in \mathbb{N}\} \text{ (\alpha-entropy)}, \\ \sum_{i=1}^N \{p_{\theta,i}(C) \log p_{\theta,i}(C) + (1 - p_{\theta,i}(C)) \log(1 - p_{\theta,i}(C))\} & \text{(cross-entropy)}, \end{cases}$$

where $\gamma \in \mathbb{R}$ represents a penalty parameter. Then they anneal the penalty parameter from high $\gamma > 0$ to $\gamma \approx 0$ to smooth the non-convexity of the objective function $\hat{l}(\theta; C, \lambda)$ similar to simulated annealing [Kirkpatrick et al., 1983].

To address the rounding issue, Ichikawa [2023] further annealed the entropy term to $\gamma \leq 0$ until the entropy term approaches zero, i.e., $s(\theta, C) \approx 0$, enforcing the relaxed variable to be a discrete variable and further smoothing the continuous loss landscape for optimal discrete solutions. This method is referred to as continuous relaxation annealing (CRA) and the solver that applies the CRA to the PI-GNN solver is referred to as the CRA-PI-GNN solver. When performing annealing in the direction of $\gamma < 0$, it is crucial to use the α -entropy because the gradient of the cross-entropy term diverges near 0 and 1, making learning challenging without other techniques, e.g. gradient clipping.

3 Continuous Tensor Relaxation Annealing for UL-based Solver

In this section, we first generalize CRA to CTRA, which enables UL-based solvers to efficiently solve multiple problems in a single run. Then, we extend CTRA to the tasks finding penalty-diversified and variation-diversified solutions.

Continuous tensor relaxation strategy We consider solving multiple instances $\mathcal{C}_S = \{C_s \mid C_s \in \mathcal{C}\}_{1 \leq s \leq S}$, each with different penalty parameters $\Lambda_S = \{\lambda_s\}_{1 \leq s \leq S}$ simultaneously. To achieve this, we relax a binary vector $\mathbf{x} \in \{0, 1\}^N$ into an augmented continual tensor $P \in [0, 1]^{N \times S}$ for training, and then minimize the following loss function:

$$\hat{R}(P; \mathcal{C}_S, \Lambda_S, \gamma) = \sum_{s=1}^S \hat{l}(P_{:s}; C_s, \lambda_s) + \gamma S(P), \quad S(P) \triangleq \sum_{i=1}^N \sum_{s=1}^S (1 - (2P_{is} - 1)^\alpha), \quad (6)$$

where $P_{:s} \in [0, 1]^N$ denotes each column vector of the continuous matrix P , i.e. $P = (P_{:s})_{1 \leq s \leq S} \in [0, 1]^{N \times S}$. When \hat{R} is optimized, each column $P_{:s}$ is to minimize each objective function $\hat{l}(P_{:s}; C_s, \lambda_s)$. Additionally, we also generalize the entropy term $s(\mathbf{p})$ in Eq. (5) into $S(P)$ for augmented continual tensor. Specifically, the following theorem holds.

Theorem 3.1. *Under the assumption that for all $s \in [S]$, each objective function $\hat{l}(P_{:s}; C_s, \lambda_s)$ is bounded within the domain $[0, 1]^N$, for all $s \in [S]$, each column solutions $P_{:s}^* \in \arg\min_P \hat{R}(P; \mathcal{C}_S, \Lambda_S, \gamma)$ converges to the corresponding original solutions $\mathbf{x}^* \in \arg\min_{\mathbf{x}} l(\mathbf{x}; C_s, \lambda_s)$ as $\gamma \rightarrow +\infty$. In addition, as $\gamma \rightarrow -\infty$, the loss function $\hat{R}(P; \mathcal{C}_S, \Lambda_S)$ becomes convex and has the soft solution $\mathbf{1}_N \mathbf{1}_S^\top / 2 = \arg\min_P \hat{R}(P; \mathcal{C}_S, \Lambda_S, \gamma)$ is unique.*

Refer to Appendix A.1 for the detailed proof. The relaxation approach has the potential for further extension to higher-order tensors, $P \in [0, 1]^{N \times S_1 \times \dots}$ which has the potential to more effectively utilize the GPU. Investigating this implementation presents a interesting direction for future research endeavors. For UL-based solvers, we parameterize the soft tensor solution as follows:

$$\hat{R}(\theta; \mathcal{C}_S, \Lambda_S, \gamma) = \sum_{s=1}^S \hat{l}(\theta; C_s, \lambda_s) + \gamma S(\theta; \mathcal{C}_S), \quad S(\theta; \mathcal{C}_S) \triangleq \sum_{i=1}^N \sum_{s=1}^S (1 - (2P_{\theta, is}(C_s) - 1)^\alpha), \quad (7)$$

where this γ is also annealed from positive to negative, similar to CRA-PI-GNN solver in Section 2. Following the UL-based solvers [Karalias and Loukas, 2020, Schuetz et al., 2022b, Ichikawa, 2023], this study characterizes P_θ using a GNN. In this study, the solver that applies the CTRA to the PI-GNN solver is referred to as the CTRA-PI-GNN solver. Furthermore, in this study, even when addressing multiple problems using Eq. (7), the network structure, except for the output layer, employs the same architecture as the GNN used in PI-GNN and CRA-PI-GNN [Schuetz et al., 2022a, Ichikawa, 2023] that output a single solution for a single instance. When handling the similar S instances, only the output of final layer changes from 1 to S , and only the number of parameters in the final layer linearly increases by a factor of S , which is both memory and cost-efficient, and the training runtime remains nearly identical to when handling a single problem as discussed in following numerical experiments. For a more detailed explanation of the GNN and the specific network structure, refer to Appendix C.1. Additionally, by employing the simple technique of keeping network size except for the output layer, GNNs more actively learns common representations among the problems like the bottleneck

structure of autoencoder, and automatically executes efficient parallel processing. Indeed, numerical experiments demonstrated that this learning of common representations among problems leads to better solutions compared to the single-solution solver. In Appendix D.5, we provide examples demonstrating the capability of solving multiple problems with similar structures more efficiently and effectively than the CRA-PI-GNN. However, since this paper focuses on acquiring diverse solutions, the extent to which similar problems can be solved quickly remains a topic for future work.

CTRA for penalty-diversified solutions To finding penalty-diversified solutions, we aim to minimize the following loss function, which is a special case of Eq. (7):

$$\hat{R}(\boldsymbol{\theta}; C, \Lambda_S, \gamma) = \sum_{s=1}^S \hat{l}(\boldsymbol{\theta}; C, \boldsymbol{\lambda}_s) + \gamma S(\boldsymbol{\theta}; C_S). \quad (8)$$

By solving this optimization problem, for all $s \in [S]$ each column $P_{\boldsymbol{\theta},:s}(C_s)$ corresponds to the optimal solution for the penalty parameters $\boldsymbol{\lambda}_s$. In the case of penalty-diversified solutions, the variation in each s is primarily limited to the penalty coefficient of the problem, resulting in a significant correlation among instances. From the previous discussion, CTRA learns this common structure and automatically executes efficient parallelization.

CTRA for variation-diversified solutions Next, for the exploration of variation-diversified solutions to a single instance C and a penalty parameter $\boldsymbol{\lambda}$, we introduce a diversity penalty into Eq. (7) as follows:

$$\hat{R}(\boldsymbol{\theta}; C, \boldsymbol{\lambda}, \gamma, \nu) = \sum_{s=1}^S \hat{l}(\boldsymbol{\theta}; C, \boldsymbol{\lambda}) + \gamma S(\boldsymbol{\theta}; C_s) + \nu \Psi(\boldsymbol{\theta}; C), \quad (9)$$

$$\Psi(\boldsymbol{\theta}; C) = -S \sum_{i=1}^N \text{STD} [\{P_{\boldsymbol{\theta},is}(C)\}_{1 \leq s \leq S}], \quad (10)$$

where, $\Psi(\boldsymbol{\theta}; C, \nu)$ acts as a constraint term to induce diversity in each column $P_{\boldsymbol{\theta},:s}(C)$, and ν is the parameter controlling the intensity of this constraints. Setting ν to 0 in Eq. (9) almost corresponds to tackling the same CO problem with different initial conditions. The following proposition shows that this diversity measure $\Psi(\boldsymbol{\theta}; C)$ is a natural relaxation of the diversity metric in CO problems, known to max sum hamming distance [Fomin et al., 2020, 2023, Baste et al., 2022, 2019].

Proposition 3.2. For binary sequences $\{\boldsymbol{x}_s\}_{s=1}^S, \forall s, \boldsymbol{x}_s \in \{0, 1\}^N$, following equality holds

$$S^2 \sum_{i=1}^N \text{VAR} [\{\boldsymbol{x}_{s,i}\}_{1 \leq s \leq S}] = \sum_{s < l} d_H(\boldsymbol{x}_s, \boldsymbol{x}_l). \quad (11)$$

where the right-hand side of Eq. (11) is the max sum hamming distance.

Refer to Appendix A.2 for the detailed proof. Note that the Eq. (11) not only naturally relaxes the max sum hamming distance but also reduces the number of sums related to the parallel number S from $\mathcal{O}(S^2)$ in the case of the max sum Hamming distance to $\mathcal{O}(S)$ in the case of the diversity penalty. Thus, as S increases, the latter allows for significantly faster gradient computation. This study use standard deviation in Eq. 9 to match scaling of other terms.

4 Related work

The computation of penalty-diversified solutions is straightforward and can be easily parallelized if we have k times the computational resources. On the other hand, variation-diversified solutions are non-trivial, and many studies have been done on this topic. A common approach is to select k solutions that maximize a diversity measure [Fernau et al., 2019], which is typically based on the Hamming distance. Traditionally, in areas such as graph algorithms [Baste et al., 2019, 2022, Hanaka et al., 2021], constraint programming [Hebrard et al., 2005, Petit and Trapp, 2015], and mathematical programming [Danna et al., 2007, Danna and Woodruff, 2009, Petit and Trapp, 2019], there are two known problem settings [Hebrard et al., 2005]: offline diversity problems, where the entire set of solutions is computed at once, and online diversity problems, where solutions are computed

Table 1: The objective functions for the three problems to be studied.

	Objective Function	Parameters
MIS	$l(\mathbf{x}; G, \lambda) = -\sum_{i \in V} x_i + \lambda \sum_{(i,j) \in E} x_i x_j$	$ V = N$
MaxCut	$l(\mathbf{x}; G) = \sum_{i < j} A_{ij}(2x_i x_j - x_i - x_j)$	$A \in \mathbb{R}^{N \times N}$
DBM	$l(\mathbf{x}; C = \{A, M\}, \boldsymbol{\lambda}) = -\sum_{ij} A_{ij} x_{ij} + \lambda_1 \sum_i \text{ReLU}(\sum_j x_{ij} - 1) + \lambda_2 \sum_j \text{ReLU}(\sum_i x_{ij} - 1) + \lambda_3 \text{ReLU}(p \sum_{ij} x_{ij} - \sum_{ij} M_{ij} x_{ij}) + \lambda_4 \text{ReLU}(q \sum_{ij} x_{ij} - \sum_{ij} (1 - M_{ij}) x_{ij})$	$A \in \mathbb{R}^{N_1 \times N_2}$ $M \in \mathbb{R}^{N_1 \times N_2}$ $p, q \in \mathbb{R}$

incrementally. Offline methods often require enumerating a large number of solutions, many of which are similar, leading to inefficiency and lack of scalability. Online methods, due to their sequential nature, are time-consuming, cannot be parallelized, and are prone to getting stuck in local optima. To address these limitations, we focus on methods that simultaneously compute k high-quality solutions while maximizing the diversity measure. For example, solvers based on evolutionary algorithms are one such method [Deb, 2001]. Our approach is different, using a UL-based solver that takes advantage of efficient GPU-driven parallel processing and is capable of handling large-scale problems.

5 Experiments

This section evaluate the effectiveness of CTRA-PI-GNN solver in discovering penalty-diversified and variation-diversified solutions across three CO problems: the maximum independent set (MIS), maximum cut (MaxCut), diverse bipartite problems (DBM) problems. Their objective functions are summarized in Table 1. For the detailed explanation, refer to Appendix C.3.

5.1 Settings

Baseline Our baseline include the results from executing a greedy algorithms and PI-GNN solver [Schuetz et al., 2022a] and CRA-PI-GNN solver [Ichikawa, 2023] multiple times. These solvers are run multiple times with with different penalty parameters for penalty-diversified solutions and different random seeds for variation-diversified solutions, allowing us to evaluate the search efficiency for both types of diversified solutions. For the MIS problem, we employ a random greedy search implemented by NetworkX, and for the MaxCut problem, we use a random greedy search implemented by Mehta [2019]. While there are some online heuristics for exploring variation-diversified solutions by generating solutions distant from those already obtained, these methods are not included as benchmarks due to their inefficiency in utilizing GPUs and their poor scalability to large problems. We track the runtime t of each execution, from the model training to obtaining the final output.

Implementation The objective of this numerical experiment is to validate that CTRA can obtain penalty-diversified and variation-diversified solutions with a comparable number of parameters and runtime to UL-based solvers that output a single solution, as described in Section 3. Therefore, in our experiments, CTRA-PI-GNN solver employs the same network architecture as PI-GNN [Schuetz et al., 2022a] and CRA-PI-GNN [Ichikawa, 2023] solvers, except for the output size of the final layer. We use GraphSage implemented with Deep Graph Library [Wang et al., 2019]. Detailed architectures of these GNNs can be found in Appendix C.1. We use the AdamW [Kingma and Ba, 2014] optimizer with a learning rate of $\eta = 10^{-4}$ and weight decay of 10^{-2} . The GNNs are trained for up to 5×10^4 epochs with early stopping, which monitors the summarized loss function $\sum_{s=1}^S \hat{l}(P_{:,s})$ and the entropy term $\Phi(P; \gamma, \alpha)$ with tolerance 10^{-5} and patience 10^3 epochs; Further details are provided in Appendix C.2. We set the initial scheduling value as $\gamma(0) = -20$ for the MIS and DBM problems and $\gamma(0) = -6$ for the MaxCut problems, with same scheduling rate $\varepsilon = 10^{-3}$ and curvature rate $\alpha = 2$ in Eq. (7).

Evaluation metrics Following the metric of Wang and Li [2023], we employ the approximation rate (ApR) for all experiments, defined by $\text{ApR} = f(\mathbf{x}; C) / f(\mathbf{x}^*; C)$, where \mathbf{x}^* denotes optimal solutions. For MIS, these optimal solutions set to the theoretical results [Barbier et al., 2013], for DBM problems, they are identified using Gurobi 10.0.1 solver with default settings, and for

MIS ($d = 5$)			
Method {#Runs}	#Params	Time (s)	ApR*
PI-GNN {20}	$5,022,865 \times 20$	$13,189 \pm 60$	0.883 ± 0.002
CRA {20}	$5,022,865 \times 20$	$14,400 \pm 42$	0.961 ± 0.002
CTRA {1}	5,083,076	1,194 \pm 8	0.934 ± 0.002

MIS ($d = 20$)			
Method {#Runs}	#Params	Time (s)	ApR*
PI-GNN {20}	$5,022,865 \times 20$	$15,191 \pm 24$	0.759 ± 0.007
CRA {20}	$5,022,865 \times 20$	$14,816 \pm 40$	0.928 ± 0.004
CTRA {1}	5,083,076	1,254 \pm 10	0.878 ± 0.011

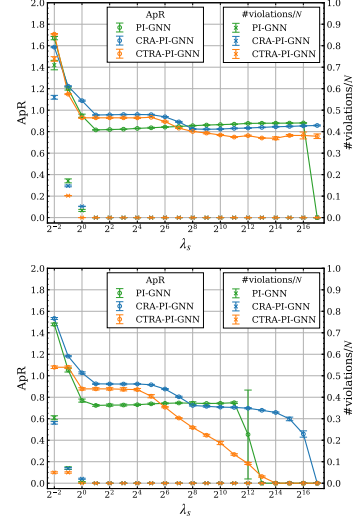


Figure 2: (Left Table) shows runtime (Time), number of parameters (#Params), and maximum ApR (ApR*) for each method. (Right Figure) shows ApRs across different penalty parameters Λ_s . Error represent the standard deviations of 5 random seeds. CTRA-PI-GNN solver can find penalty-diversified solutions in a single run with a comparable #Params and runtime to UL-based solvers that output a single solution.

MaxCut problems, they are the best-known solutions. To evaluate the quality of penalty-diversified solutions, we assess $\text{ApR}^* = \max_{s \in [S]} (\text{ApR}(\mathbf{x}_s))$ in relation to the parallel number S in Eq. (7). For assessing the quality of variation-diversified solutions, we assess the average ApR, defined as $\bar{\text{ApR}} = \sum_{s=1}^S \text{ApR}_s / S$, and define a diverse Score (DScore) for the bit sequences $\{\mathbf{x}_s\}_{s=1}^S$:

$$\text{DScore}(\{\mathbf{x}_s\}_{s=1}^S) = \frac{2}{NS(S-1)} \sum_{s < l} d_H(\mathbf{x}_s, \mathbf{x}_l). \quad (12)$$

A higher DScore indicates greater variation among solutions. The desired properties of a variation-diversified solution include both a reasonably good quality of solutions and a diverse set of solutions with different characteristics. Thus, solutions with higher values of both average ApR and DScore exhibit more favorable properties. All the results for MIS are summarized based on 5 RRGs with different random seeds.

5.2 Finding penalty-diversified Solutions

MIS problems First, we compare the performance of CTRA-PI-GNN for MIS problems on RRGs, $G(V, E)$, with $|V| = 10,000$ nodes and the node degree of 5 and 20. CTRA-PI-GNN solver run using Eq. 8, with a set of penalty parameters, $\Lambda_S = \{2^{s-3} \mid s = 1, \dots, 20\}$. CRA-PI-GNN and PI-GNN solver run multiple times for each penalty parameter $\lambda_s \in \Lambda_S$. Fig. 2 (Right) shows the ApR as a function of penalty parameters $\lambda_s \in \Lambda_S$. Across all penalty parameters, from 2^{-2} to 2^{16} , CTRA-PI-GNN solver performs on par with or slightly underperforms CRA-PI-GNN solver. Table in Fig. 2 (Right) shows the runtime and number of parameters (#Params) for CTRA-PI-GNN solver at $S = 20$, compared to the total runtime and #Params for S multiple runs of PI-GNN and CRA-PI-GNN solvers. These result indicate that CTRA-PI-GNN solver can find penalty-diversified solutions with a comparable number of parameters and runtime to UL-based solvers that output a single solution. For a more detailed discussion on the dependence of the runtime and the #params for number of shot S , refer to Appendix D.1.

DBM problems We next demonstrate the effectiveness of CTRA-PI-GNN solver for DBM problems, which serve as practical CO problems. We focus on the first of 27 DBM instances; see Appendix D.6 for the results of other instances except for the first. Given that (λ_1, λ_2) and (λ_3, λ_4) share similar properties, CTRA-PI-GNN run with a set of $S = 11 \times 11$ parameters on the a grid, $\Lambda_S = \{\lambda_s = (\lambda_a, \lambda_b, \lambda_c, \lambda_d)\}$, where $\lambda_a, \lambda_b \in \{2^s \mid s = 0, \dots, 10\}$. CRA-PI-GNN and PI-GNN

DBM instance-1, matching-1			
Method {#Runs}	#Params	Time (s)	ApR*
PI-GNN {121}	$12,507,501 \times 121$	$45,000 \pm 5,778$	0.883 ± 0.040
CRA {121}	$12,507,501 \times 121$	$213,612 \pm 5,132$	1.000 ± 0.000
CTRA {1}	$13,107,621$	$1,961 \pm 101$	0.883 ± 0.011

DBM instance-1, matching-2			
Method {#Runs}	#Params	Time (s)	ApR*
PI-GNN {121}	$12,507,501 \times 121$	$28,064 \pm 7,105$	0.927 ± 0.024
CRA {121}	$12,507,501 \times 121$	$208,141 \pm 903$	0.990 ± 0.013
CTRA {1}	$13,107,621$	$2,154 \pm 164$	1.000 ± 0.000

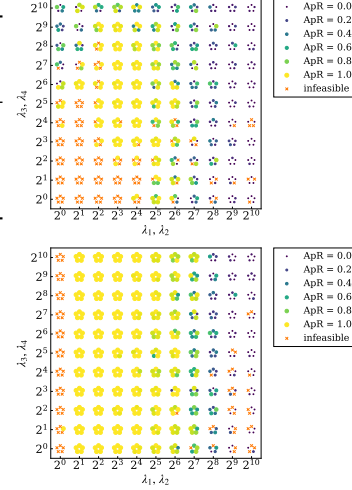


Figure 3: (Left Table) shows runtime (Time), number of parameters (#Params), and maximum ApR (ApR*) for each method, with errors representing the standard deviations of 5 random seeds. (Right Figure) shows ApRs, where each point represents the results from 5 random seed across various penalty parameters $\Lambda_S = \{\lambda_s = (\lambda_a, \lambda_b) \mid \lambda_a, \lambda_b \in \{2^s \mid s = 0, \dots, 10\}\}$. CTRA-PI-GNN solver is capable of finding penalty-diversified solutions in a single run, with a comparable number of parameters and runtime to those of UL-based solvers.

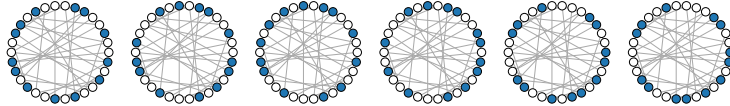


Figure 4: The obtained solutions by CTRA-PI-GNN solver for the MIS problem on a RRG with 30 nodes and the degree $d = 3$. Blue nodes represent the independent set.

solver run multiple times for each penalty parameter $\lambda_s \in \Lambda_S$ Fig. 3 (Right) shows that the ApR on the grid Λ_S using the CTRA-PI-GNN solver identifies a desirable region where the ApR is nearly 1.0. Table in Fig. 3 (Left) demonstrates that CTRA-PI-GNN solver can find penalty-diversified solutions with a comparable number of parameters and runtime to UL-based solvers that output a single solution.

5.3 Finding variation-diversified solutions

MIS problems We first run CTRA-PI-GNN solver using Eq. (9) to find variation-diversified solutions for MIS problems on small-scaled RRGs with 30 nodes and the node degree set to 3. We set the parameter $\nu = 0.5$ and the number of shots $S = 100$ in Eq. (9). As shown in Fig. 4, CTRA-PI-GNN solver can successfully obtain 6 solutions with 13 independent sets, which is the global optimum value. We extend the investigation to large-scale RRG with 10,000 nodes and a node degree $d = 20$, which is known for its optimization challenges [Angelini and Ricci-Tersenghi, 2023]. These experiments examine the parameter ν dependency of quality of variation-diversified solutions with a fixed number of shots $S = 300$. Fig. 5 (Right) shows the low dimensional solutions using a 2 dimensional mapping of normalized solutions $\{P_{:,s}\}_{s=1}^{300}$ using principal component analysis (PCA), selecting the two principal components with the highest contribution rates for different parameters $\nu = 0.0, 0.2, 0.4, 0.6$. These results indicate that by increasing parameter ν , diverse solutions can be obtained in the high-contribution space where the solution space is getting be separated. The table in Fig. 5 measures the time, ApR, and DScore when the parallel execution number $S = 300$ is run with different random seeds. The results show that although the time of CTRA-PI-GNN solver is slower compared to executing the greedy algorithm multiple times, both ApR and DScore reach their maximum at $\nu = 0.2$, resulting in the highest quality variation-diversified solutions. Additionally, increasing parameter ν enhances the exploration capability of GNN, leading to better solutions compared to conventional PI-GNN and CRA-PI-GNN; see Appendix D.2.

Method {#Runs}	MIS ($d = 20$)		
	Time (s)	$\overline{\text{ApR}}$	DScore
Greedy {300}	8	0.715	0.239
PI-GNN {300}	13,498	0.712	0.238
CRA {300}	15,136	0.923	0.248
CTRA ($\nu = 0.0$) {1}	95	0.873	0.019
CTRA ($\nu = 0.2$) {1}	154	0.936	0.260
CTRA ($\nu = 0.4$) {1}	154	0.900	0.251
CTRA ($\nu = 0.6$) {1}	149	0.852	0.257

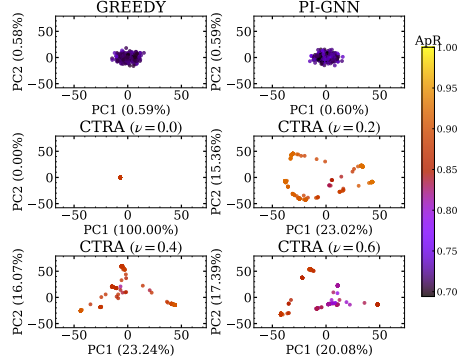


Figure 5: (Left Table) shows runtime (Time), average ApR ($\overline{\text{ApR}}$), DScore for each method on MIS problems with a node degree $d = 20$. (Right Figure) shows the distribution of solutions in a 2-dimensional space using PCA with varying ν .

Method {#Runs}	MaxCut G14		
	Time (s)	$\overline{\text{ApR}}$	DScore
Greedy {1,000}	87	0.936	0.479
PI-GNN {1,000}	25,871	0.963	0.499
CRA {1,000}	48,639	0.988	0.499
CTRA ($\nu = 0.0$) {1}	144	0.977	0.497
CTRA ($\nu = 0.4$) {1}	138	0.991	0.501
CTRA ($\nu = 0.8$) {1}	141	0.989	0.501
CTRA ($\nu = 1.2$) {1}	147	0.985	0.502

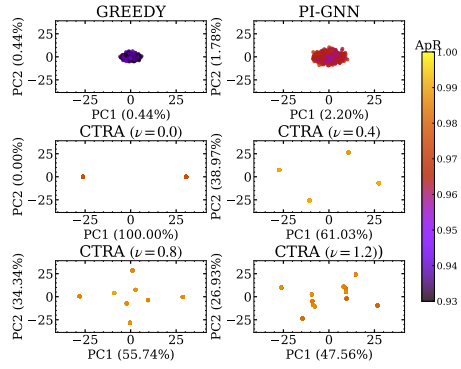


Figure 6: (Left Table) shows runtime (Time), average ApR ($\overline{\text{ApR}}$), DScore for each method on MaxCut G14, with error representing the standard deviations of 5 random seeds. (Right Figure) shows the distribution of solutions in a 2-dimensional space using PCA with varying ν .

MaxCut problem We next evaluate the ability to find variation-diversified solutions in the G14 instance in the Gset, which has many 4-clustered solution space. We set the number of shot $S = 1,000$ in Eq. (9). Fig. 6 (Right) demonstrates that CTRA-PI-GNN solver can capture 4-clustered solutions beyond a value of ν . Table in Fig. 6 measures the time, $\overline{\text{ApR}}$, and DScore when the parallel execution number $S = 1,000$ is run with different random seeds. The results show that although the runtime of CTRA-PI-GNN solver is slower compared to executing the greedy algorithm multiple times, $\overline{\text{ApR}}$ and DScore reach their maximum at $\nu = 0.4$ and $\nu = 1.2$, respectively. Additionally, as well as MIS problems, enhancement of the exploration is consistent across various Gset. For further details; see Appendix D.3.

6 Conclusion

This study introduces the Continual Tensor Relaxation Annealing (CTRA) framework for unsupervised learning (UL)-based solvers, designed to efficiently find both penalty-diversified and variation-diversified solutions within a single training session. CTRA utilizes the power of representation learning to automatically and efficiently learn shared representations and enable effective parallelization. Our numerical experiments validate that CTRA can discover penalty-diversified and variation-diversified solutions with a comparable number of parameters and runtime to conventional UL-based solvers that generate only a single solution. This approach not only enhances the computational efficiency for finding these diversified solutions but also improves the search capabilities, resulting in higher-quality solutions compared to existing UL-based solvers that output a single solution and greedy algorithms.

References

- Christos H Papadimitriou and Kenneth Steiglitz. *Combinatorial optimization: algorithms and complexity*. Courier Corporation, 1998.
- Bernhard H Korte, Jens Vygen, B Korte, and J Vygen. *Combinatorial optimization*, volume 1. Springer, 2011.
- Tiago Pereira, Maryam Abbasi, Bernardete Ribeiro, and Joel P Arrais. Diversity oriented deep reinforcement learning for targeted molecule generation. *Journal of cheminformatics*, 13(1):21, 2021.
- Martin JA Schuetz, J Kyle Brubaker, and Helmut G Katzgraber. Combinatorial optimization with physics-inspired graph neural networks. *Nature Machine Intelligence*, 4(4):367–377, 2022a.
- Nikolaos Karalias and Andreas Loukas. Erdos goes neural: an unsupervised learning framework for combinatorial optimization on graphs. *Advances in Neural Information Processing Systems*, 33: 6659–6672, 2020.
- Haoyu Peter Wang, Nan Wu, Hang Yang, Cong Hao, and Pan Li. Unsupervised learning for combinatorial optimization with principled objective relaxation. *Advances in Neural Information Processing Systems*, 35:31444–31458, 2022.
- Haoyu Wang and Pan Li. Unsupervised learning for combinatorial optimization needs meta-learning. *arXiv preprint arXiv:2301.03116*, 2023.
- Martin JA Schuetz, J Kyle Brubaker, Zhihuai Zhu, and Helmut G Katzgraber. Graph coloring with physics-inspired graph neural networks. *Physical Review Research*, 4(4):043131, 2022b.
- Yuma Ichikawa. Controlling continuous relaxation for combinatorial optimization. *arXiv preprint arXiv:2309.16965*, 2023.
- Haoran Sun, Etash K Guha, and Hanjun Dai. Annealed training for combinatorial optimization on graphs. *arXiv preprint arXiv:2207.11542*, 2022.
- Sebastian Sanokowski, Wilhelm Berghammer, Sepp Hochreiter, and Sebastian Lehner. Variational annealing on graphs for combinatorial optimization. *Advances in Neural Information Processing Systems*, 36, 2024.
- Scott Kirkpatrick, C Daniel Gelatt Jr, and Mario P Vecchi. Optimization by simulated annealing. *science*, 220(4598):671–680, 1983.
- Fedor V Fomin, Petr A Golovach, Lars Jaffke, Geevarghese Philip, and Danil Sagunov. Diverse pairs of matchings. *arXiv preprint arXiv:2009.04567*, 2020.
- Fedor V Fomin, Petr A Golovach, Fahad Panolan, Geevarghese Philip, and Saket Saurabh. Diverse collections in matroids and graphs. *Mathematical Programming*, pages 1–33, 2023.
- Julien Baste, Michael R Fellows, Lars Jaffke, Tomáš Masařík, Mateus de Oliveira Oliveira, Geevarghese Philip, and Frances A Rosamond. Diversity of solutions: An exploration through the lens of fixed-parameter tractability theory. *Artificial Intelligence*, 303:103644, 2022.
- Julien Baste, Lars Jaffke, Tomáš Masařík, Geevarghese Philip, and Günter Rote. Fpt algorithms for diverse collections of hitting sets. *Algorithms*, 12(12):254, 2019.
- Henning Fernau, Petr Golovach, Marie-France Sagot, et al. Algorithmic enumeration: Output-sensitive, input-sensitive, parameterized, approximative (dagstuhl seminar 18421). In *Dagstuhl Reports*, volume 8. Schloss Dagstuhl-Leibniz-Zentrum fuer Informatik, 2019.
- Tesshu Hanaka, Yasuaki Kobayashi, Kazuhiro Kurita, and Yota Otachi. Finding diverse trees, paths, and more. In *Proceedings of the AAAI Conference on Artificial Intelligence*, volume 35, pages 3778–3786, 2021.
- Emmanuel Hebrard, Brahim Hnich, Barry O’ Sullivan, and Toby Walsh. Finding diverse and similar solutions in constraint programming. In *AAAI*, volume 5, pages 372–377, 2005.

- Thierry Petit and Andrew C Trapp. Finding diverse solutions of high quality to constraint optimization problems. In *IJCAI. International Joint Conference on Artificial Intelligence*, 2015.
- Emilie Danna, Mary Fenelon, Zonghao Gu, and Roland Wunderling. Generating multiple solutions for mixed integer programming problems. In *International Conference on Integer Programming and Combinatorial Optimization*, pages 280–294. Springer, 2007.
- Emilie Danna and David L Woodruff. How to select a small set of diverse solutions to mixed integer programming problems. *Operations Research Letters*, 37(4):255–260, 2009.
- Thierry Petit and Andrew C Trapp. Enriching solutions to combinatorial problems via solution engineering. *INFORMS Journal on Computing*, 31(3):429–444, 2019.
- Kalyanmoy Deb. *Multi-objective optimization using evolutionary algorithms*, volume 16. John Wiley & Sons, 2001.
- Hermish Mehta. Cvx graph algorithms. <https://github.com/hermish/cvx-graph-algorithms>, 2019.
- Minjie Wang, Da Zheng, Zihao Ye, Quan Gan, Mufei Li, Xiang Song, Jinjing Zhou, Chao Ma, Lingfan Yu, Yu Gai, et al. Deep graph library: A graph-centric, highly-performant package for graph neural networks. *arXiv preprint arXiv:1909.01315*, 2019.
- Diederik P Kingma and Jimmy Ba. Adam: A method for stochastic optimization. *arXiv preprint arXiv:1412.6980*, 2014.
- Jean Barbier, Florent Krzakala, Lenka Zdeborová, and Pan Zhang. The hard-core model on random graphs revisited. In *Journal of Physics: Conference Series*, volume 473, page 012021. IOP Publishing, 2013.
- Maria Chiara Angelini and Federico Ricci-Tersenghi. Modern graph neural networks do worse than classical greedy algorithms in solving combinatorial optimization problems like maximum independent set. *Nature Machine Intelligence*, 5(1):29–31, 2023.
- Justin Gilmer, Samuel S Schoenholz, Patrick F Riley, Oriol Vinyals, and George E Dahl. Neural message passing for quantum chemistry. In *International conference on machine learning*, pages 1263–1272. PMLR, 2017.
- Franco Scarselli, Marco Gori, Ah Chung Tsoi, Markus Hagenbuchner, and Gabriele Monfardini. The graph neural network model. *IEEE transactions on neural networks*, 20(1):61–80, 2008.
- Richard M Karp. *Reducibility among combinatorial problems*. Springer, 2010.
- Mohsen Bayati, David Gamarnik, and Prasad Tetali. Combinatorial approach to the interpolation method and scaling limits in sparse random graphs. In *Proceedings of the forty-second ACM symposium on Theory of computing*, pages 105–114, 2010.
- Amin Coja-Oghlan and Charilaos Efthymiou. On independent sets in random graphs. *Random Structures & Algorithms*, 47(3):436–486, 2015.
- Aaron Ferber, Bryan Wilder, Bistra Dilkina, and Milind Tambe. Mipaal: Mixed integer program as a layer. In *Proceedings of the AAAI Conference on Artificial Intelligence*, volume 34, pages 1504–1511, 2020.
- Maxime Mulamba, Jayanta Mandi, Michelangelo Diligenti, Michele Lombardi, Victor Bucarey, and Tias Guns. Contrastive losses and solution caching for predict-and-optimize. *arXiv preprint arXiv:2011.05354*, 2020.
- Jayanta Mandi, Victor Bucarey, Maxime Mulamba Ke Tchomba, and Tias Guns. Decision-focused learning: through the lens of learning to rank. In *International Conference on Machine Learning*, pages 14935–14947. PMLR, 2022.
- Prithviraj Sen, Galileo Namata, Mustafa Bilgic, Lise Getoor, Brian Galligher, and Tina Eliassi-Rad. Collective classification in network data. *AI magazine*, 29(3):93–93, 2008.

Bahram Alidaee, Gary A Kochenberger, and Ahmad Ahmadian. 0-1 quadratic programming approach for optimum solutions of two scheduling problems. *International Journal of Systems Science*, 25(2):401–408, 1994.

Hartmut Neven, Georgie Rose, and William G Macready. Image recognition with an adiabatic quantum computer i. mapping to quadratic unconstrained binary optimization. *arXiv preprint arXiv:0804.4457*, 2008.

Michel Deza and Monique Laurent. Applications of cut polyhedra—ii. *Journal of Computational and Applied Mathematics*, 55(2):217–247, 1994.

Y. Ye. The gset dataset. <https://web.stanford.edu/~yye/yye/Gset/>, 2003.

A Derivations

A.1 Proof of Theorem 3.1

Following the proof of Ichikawa [2023], we show Theorem A.4 based on following three lemmas.

Lemma A.1. *For any even natural number $\alpha = 2, 4, \dots$, the function $\phi(p) = 1 - (2p - 1)^\alpha$ defined on $[0, 1]$ achieves its maximum value of 1 when $p = 1/2$ and its minimum value of 0 when $p = 0$ or $p = 1$.*

Proof. The derivative of $\phi(p)$ relative to p is $\phi'(p) = -2\alpha(2p - 1)$, which is zero when $p = 1/2$. This is a point where the function is maximized because the second derivative $\phi''(p) = -4\alpha \leq 0$. In addition, this function is concave and symmetric relative to $p = 1/2$ because α is an even natural number, i.e., $\phi(p) = \phi(1 - p)$, thereby achieving its minimum value of 0 when $p = 0$ or $p = 1$. \square

Lemma A.2. *For any even natural number $\alpha = 2, 4, \dots$ and a matrix $P \in [0, 1]^{N \times S}$, if $\lambda \rightarrow +\infty$, minimizing the penalty term $\Phi(P; \gamma) = \gamma \sum_{s=1}^S \sum_{i=1}^N (1 - (2P_{is} - 1)^\alpha) = \gamma \sum_{s=1}^S \sum_{i=1}^N \phi(P_{is}; \alpha)$ enforces that the components of P_{is} must be either 0 or 1 and, if $\gamma \rightarrow -\infty$, the penalty term enforces $P = \mathbf{1}_N \mathbf{1}_N^\top / 2$.*

Proof. From Lemma B1, as $\gamma \rightarrow +\infty$, the case where $\phi(P_{is})$ becomes minimal occurs when, for each i, s , $p_{is} = 0$ or $p_i = 1$. In addition, as $\gamma \rightarrow -\infty$, the case where $\phi(p; \gamma)$ is minimized occurs when, for each i , P_{is} reaches its maximum value with $P_{is} = 1/2$. \square

Lemma A.3. $\Phi(P; \gamma) = \gamma \sum_{s=1}^S \sum_{i=1}^N (1 - (2p_i - 1)^\alpha) = \gamma \sum_{s=1}^S \sum_{i=1}^N \phi(p_i; \alpha)$ is concave when λ is positive and is a convex function when λ is negative.

Proof. Note that $\Phi(P; \gamma) = \gamma \sum_{s=1}^S \sum_{i=1}^N \phi(P_{is}; \alpha) = \gamma \sum_{i=1}^N (1 - (2P_{is} - 1)^\alpha)$ is separable across its components P_{is} . Thus, it is sufficient to prove that each $\gamma \phi(P_{is}; \alpha)$ is concave or convex in P_{is} because the sum of the concave or convex functions is also concave (and vice versa). Therefore, we consider the second derivative of $\gamma \phi_i(P_{is}; \alpha)$ with respect to P_{is} :

$$\gamma \frac{d^2 \phi_i(P_{is}; \alpha)}{dP_{is}^2} = -4\gamma\alpha$$

Here, if $\gamma > 0$, the second derivative is negative for all $p_i \in [0, 1]$, and this completes the proof that $\Phi(P; \gamma, \alpha)$ is a concave function when γ is positive over the domain $\mathbf{p} \in [0, 1]^N$. \square

Theorem A.4. *Under the assumption that the objective function $\sum_s \hat{l}(P_{:s}; C_s, \boldsymbol{\lambda}_s)$ is bounded within the domain $[0, 1]^{N \times S}$, for any $S \in \mathbb{N}$, $C_s \in \mathcal{C}_S$ and $\boldsymbol{\lambda}_s \in \Lambda_S$, as $\gamma \rightarrow +\infty$, each column $P_{:,s}^*$ of the soft solutions $P^* \in \arg\min_P \hat{R}(P; \mathcal{C}_S, \Lambda_S, \gamma)$ converges to the original solutions $\mathbf{x}^* \in \arg\min_{\mathbf{x}} l(\mathbf{x}; C_s, \boldsymbol{\lambda}_s)$. In addition, as $\gamma \rightarrow -\infty$, the loss function $\hat{R}(P; \mathcal{C}_S, \Lambda_S)$ becomes convex and the soft solution $\mathbf{1}_N \mathbf{1}_N^\top / 2 = \arg\min_P \hat{R}(P; \mathcal{C}_S, \Lambda_S, \gamma)$ is unique.*

Proof. As $\lambda \rightarrow +\infty$, the penalty term $\Phi(P; \boldsymbol{\lambda})$ dominates the loss function $\hat{R}(\mathbf{p}; C, \boldsymbol{\lambda}, \gamma)$. According to Lemma B.2, this penalty term forces the optimal solution P^* to have components p_{is}^* that are either 0 or 1 because any nonbinary value will result in an infinitely large penalty. This effectively restricts the feasible region to the vertices of the unit hypercube, which correspond to the binary vector in $\{0, 1\}^{NS}$. Thus, as $\lambda \rightarrow +\infty$, the solutions to the relaxed problem converge to $X = \arg\min_{X \in \{0, 1\}^{N \times S}} R(X_{:,s}; C_s, \boldsymbol{\lambda}_s)$. Furthermore, $\arg\min_{X \in \{0, 1\}^{N \times S}} R(X_{:,s}; C_s, \boldsymbol{\lambda}_s)$ is separable as $\sum_{s=1}^S \arg\min_{\mathbf{x} \in \{0, 1\}^N} l(\mathbf{x}; C_s, \boldsymbol{\lambda}_s)$, which indicate that each columns $X_{:,s}^* \in \arg\min_{\mathbf{x} \in \{0, 1\}^N} l(\mathbf{x}; C_s, \boldsymbol{\lambda}_s)$. As $\lambda \rightarrow -\infty$, the penalty term $\Phi(\mathbf{p}; \alpha)$ also dominates the loss function $\hat{r}(\mathbf{p}; C, \boldsymbol{\lambda}, \gamma)$ and the $\hat{r}(\mathbf{p}; C, \boldsymbol{\lambda})$ convex function from Lemma B.3. According to Lemma B.2, this penalty term forces the optimal solution $P^* = \mathbf{1}_N \mathbf{1}_N^\top / 2$. \square

A.2 Proof of Proposition 3.2

In this section, we derive Eq. (11) in Proposition 3.2.

Proof. We first note that, for binary vectors $\mathbf{x}_s, \mathbf{x}_l \in \{0, 1\}^N$, the Hamming distance is expressed as follows:

$$d_H(\mathbf{x}_s, \mathbf{x}_l) = \sum_{i=1}^N (x_{s,i}^2 + x_{l,i}^2 - 2x_{s,i}x_{l,i}). \quad (13)$$

Based on this expression, the diversity metric $\sum_{s<l} d_H(X_{:s}, X_{:l})$ can be expanded for a binary matrix $X \in \{0, 1\}^{N \times S}$ as follows:

$$\begin{aligned} \sum_{s<l} d_H(X_{:s}, X_{:l}) &= \frac{1}{2} \left(\sum_{sl} d_H(X_{:s}, X_{:l}) - \sum_s d_H^2(X_{:s}, X_{:s}) \right) \\ &= \frac{1}{2} \sum_{i=1}^N \sum_{sl} (X_{:s,i}^2 + X_{:l,i}^2 - 2X_{:s,i}X_{:l,i}) \\ &= S \sum_i \left(\sum_s X_{:s,i}^2 - \frac{1}{S} \sum_{s,l} X_{:s,i}X_{:l,i} \right). \end{aligned}$$

On the other hand, the variance of each column in a binary matrix X can be expanded as follows:

$$\begin{aligned} S^2 \sum_{i=1}^N \text{VAR}[\{X_{s,i}\}_{1 \leq s \leq S}] &= S \sum_{i=1}^N \sum_{s'=1}^S \left(X_{:s',i} - \frac{1}{S} \sum_s X_{:s,i} \right)^2 \\ &= S \sum_{i=1}^N \sum_{s'=1}^S \left(X_{:s',i}^2 - 2X_{:s',i} \frac{1}{S} \sum_s X_{:s,i} + \frac{1}{S^2} \sum_{sl} X_{:s,i}X_{:l,i} \right) \\ &= S \sum_{i=1}^N \left(\sum_{s'} X_{:s',i}^2 - \frac{2}{S} \sum_{s',s} X_{:s',i}X_{:s,i} + \frac{1}{S} \sum_{sl} X_{:s,i}X_{:l,i} \right) \\ &= S \sum_{i=1}^N \left(\sum_{s'} X_{:s',i}^2 + \frac{1}{S} \sum_{sl} X_{:s,i}X_{:l,i} \right) \\ &= \sum_{s<l} d_H(X_{:s}, X_{:l}). \end{aligned}$$

By this, we finish the proof. \square

B Additional Implementation Details

B.1 Graph Neural Networks

A graph neural network (GNN) [Gilmer et al., 2017, Scarselli et al., 2008] is a specialized neural network for representation learning of graph-structured data. GNNs learn a vectorial representation of each node through two steps. (I) Aggregate step: This step employs a permutation-invariant function to generate an aggregated node feature. (II) Combine step: Subsequently, the aggregated node feature is passed through a trainable layer to generate a node embedding, known as ‘message passing’ or ‘readout phase.’ Formally, for given graph $G = (V, E)$, where each node feature $\mathbf{h}_v^0 \in \mathbb{R}^{N^0}$ is attached to each node $v \in V$, the GNN iteratively updates the following two steps. First, the aggregate step at each k -th layer is defined by

$$\mathbf{a}_v^k = \text{Aggregate}_\theta^k(\{h_u^{k-1}, \forall u \in \mathcal{N}_v\}), \quad (14)$$

where the neighborhood of $v \in V$ is denoted as $\mathcal{N}_v = \{u \in V \mid (v, u) \in E\}$, \mathbf{h}_u^{k-1} is the node feature of neighborhood, and \mathbf{a}_v^k is the aggregated node feature of the neighborhood. Second, the combined step at each k -th layer is defined by

$$\mathbf{h}_v^k = \text{Combine}_\theta^k(\mathbf{h}_v^{k-1}, \mathbf{a}_v^k), \quad (15)$$

where $\mathbf{h}_v^k \in \mathbb{R}^{N^k}$ denotes the node representation at k -th layer. The total number of layers, K , and the intermediate vector dimension, N^k , are empirically determined hyperparameters. Although numerous implementations for GNN architectures have been proposed, the most basic and widely used GNN architecture is a graph convolutional network (GCN) [Scarselli et al., 2008] given by

$$\mathbf{h}_v^k = \sigma \left(W^k \sum_{u \in \mathcal{N}(v)} \frac{\mathbf{h}_u^{k-1}}{|\mathcal{N}(v)|} + B^k \mathbf{h}_v^{k-1} \right), \quad (16)$$

where W^k and B^k are trainable parameters, $|\mathcal{N}(v)|$ serves as normalization factor, and $\sigma : \mathbb{R}^{N^k} \rightarrow \mathbb{R}^{N^k}$ is some component-wise nonlinear activation function such as sigmoid or ReLU function.

C Experiment Details

This section describes the details of the experiments .

C.1 Architecture of GNNs

We describe the details of the GNN architectures used in our numerical experiments. For each node $v \in V$, the first convolutional layer takes a node embedding vectors, $\mathbf{h}_{v,\theta}^0$ for each node, yielding feature vectors $\mathbf{h}_{v,\theta}^1 \in \mathbb{R}^{H_1}$. Then, the ReLU function is used as a component-wise nonlinear transformation. The second convolutional layer takes the feature vector, \mathbf{h}_{θ}^1 , as input, producing a feature vector $\mathbf{h}_{v,\theta}^2 \in \mathbb{R}^S$. Finally, a sigmoid function is applied to the vector \mathbf{h}_{θ}^2 , producing the tensor solutions $P_{v,\theta} \in [0, 1]^{N \times S}$. Here, for MIS and MaxCut problems, we set $|H_0| = \text{int}(N^{0.8})$ as in Schuetz et al. [2022a], Ichikawa [2023], and for the DBM problems, we set it to 2,500. Across all problems, we set $H_1 = H_0$, and $H_2 = S$. We conducted all experiments by using V100GPU.

C.2 Training setting and post-rounding method

We use the AdamW [Kingma and Ba, 2014] optimizer with a learning rate as $\eta = 10^{-4}$ and weight decay as 10^{-2} . The training the GNNs conducted for a duration of up to 5×10^4 epochs with early stopping, which monitors the summarized loss function $\sum_{s=1}^S \hat{l}(P_{:,s})$ and penalty term $\Phi(P; \gamma, \alpha)$ with tolerance 10^{-5} and patience 10^3 . After the training phase, we apply projection heuristics to round the obtained soft solutions back to discrete solutions using simple projection, where for all $i \in [N]$, $s \in [S]$, we map $P_{\theta,i,s}$ to 0 if $P_{\theta,i,s} \leq 0.5$ and $P_{\theta,i,s}$ to 1 if $P_{\theta,i,s} > 0.5$. Note that due to the annealing, CTRA-PI-GNN solver ensures that the soft solution are nearly binary for all benchmarks, making them robust against the threshold 0.5 in our experiments.

C.3 Problem specification

Maximum independent set problems There are some theoretical results for MIS problems on RRGs with the node degree set to d , where each node is connected to exactly d other nodes. The MIS problem is a fundamental NP-hard problem [Karp, 2010] defined as follows. Given an undirected graph $G(V, E)$, an independent set (IS) is a subset of nodes $\mathcal{I} \in V$ where any two nodes in the set are not adjacent. The MIS problem attempts to find the largest IS, which is denoted \mathcal{I}^* . In this study, ρ denotes the IS density, where $\rho = |\mathcal{I}|/|V|$. To formulate the problem, a binary variable x_i is assigned to each node $i \in V$. Then the MIS problem is formulated as follows:

$$f(\mathbf{x}; G, \lambda) = - \sum_{i \in V} x_i + \lambda \sum_{(i,j) \in E} x_i x_j, \quad (17)$$

where the first term attempts to maximize the number of nodes assigned 1, and the second term penalizes the adjacent nodes marked 1 according to the penalty parameter λ . In our numerical experiments, we set $\lambda = 2$, following Schuetz et al. [2022a], no violation is observed as in [Schuetz et al., 2022a]. First, for every d , a specific value ρ_d^* , which is dependent on only the degree d , exists such that the independent set density $|\mathcal{I}^*|/|V|$ converges to ρ_d^* with a high probability as N approaches infinity [Bayati et al., 2010]. Second, a statistical mechanical analysis provides the typical MIS density ρ_d^{Theory} and we clarify that for $d > 16$, the solution space of \mathcal{I} undergoes a clustering

transition, which is associated with hardness in sampling [Barbier et al., 2013] because the clustering is likely to create relevant barriers that affect any algorithm searching for the MIS \mathcal{I}^* . Finally, the hardness is supported by analytical results in a large d limit, which indicates that, while the maximum independent set density is known to have density $\rho_{d \rightarrow \infty}^* = 2 \log(d)/d$, to the best of our knowledge, there is no known algorithm that can find an independent set density exceeding $\rho_{d \rightarrow \infty}^{\text{alg}} = \log(d)/d$ [Coja-Oghlan and Efthymiou, 2015].

Diverse bipartite matching (DBM) problems We adopt this CO problem from Ferber et al. [2020], Mulamba et al. [2020], Mandi et al. [2022] as a practical example. The topologies are sourced from the CORA citation network [Sen et al., 2008], where each node signifying a scientific publication, is characterized by 1,433 bag-of-words features, and the edges represents represents the likelihood of citation links. Mandi et al. [2022] focused on disjoint topologies, creating 27 distinct instances. Each instance is composed of 100 nodes, categorised into two group of 50 nodes, labeled N_1 and N_2 . The objective of DBM problems is to find the maximum matching under diversity constraints for similar and different fields. It is formulated as follows:

$$l(\mathbf{x}; C, M, \boldsymbol{\lambda}) = - \sum_{ij} C_{ij} x_{ij} + \lambda_1 \sum_{i=1}^{N_1} \text{ReLU} \left(\sum_{j=1}^{N_2} x_{ij} - 1 \right) + \lambda_2 \sum_{j=1}^{N_2} \text{ReLU} \left(\sum_{i=1}^{N_1} x_{ij} - 1 \right) + \lambda_3 \text{ReLU} \left(p \sum_{ij} x_{ij} - \sum_{ij} M_{ij} x_{ij} \right) + \lambda_4 \text{ReLU} \left(q \sum_{ij} x_{ij} - \sum_{ij} (1 - M_{ij}) x_{ij} \right), \quad (18)$$

where a reward matrix $C \in \mathbb{R}^{N_1 \times N_2}$ indicates the likelihood of a link between each node pair, for all i, j , M_{ij} is assigned 0 if articles i and j belong to the same field, or 1 if they don't. The parameters $p, q \in [0, 1]$ represent the probability of pairs being in the same field and in different fields, respectively. Following [Mandi et al., 2022], we examine two variations of this problem: Matching-1 and Matching-2, characterized by p and q values of 25% and 5%.

Maximum cut problems The MaxCut problem, a well-known NP hard problems [Karp, 2010], has practical application in machine scheduling [Alidaee et al., 1994], image recognition [Neven et al., 2008] and electronic circuit layout design [Deza and Laurent, 1994]. It is defined as follows: In an undirected graph $G = (V, E)$, a cut set $\mathcal{C} \in E$, which is a subset of edges, divides the nodes into two groups ($V_1, V_2 \mid V_1 \cup V_2 = V, V_1 \cap V_2 = \emptyset$). The objective the MaxCut problem is to find the largest cut set. To formulate this problem, each node is assigned a binary variable: $x_i = 1$ signifies that node i is in V_1 , while $x_i = 0$ indicates node i is in V_2 . For an edge (i, j) , $x_i + x_j - 2x_i x_j = 1$ is true if $(i, j) \in \mathcal{C}$; otherwise, it equal 0. This leads to the following objective function:

$$l(\mathbf{x}; G) = \sum_{i < j} A_{ij} (2x_i x_j - x_i - x_j) \quad (19)$$

where A_{ij} is the adjacency matrix, where $A_{ij} = 0$ signifies the absence of an edge, and $A_{ij} > 0$ indicates a connecting edge. Following Schuetz et al. [2022a], Ichikawa [2023], this experiments employ seven instances from Gset dataset [Ye, 2003], recognized as a standard MaxCut benchmark. These seven instances are defined on distinct graphs, including Erdős-Renyi graphs with uniform edge probability, graphs with gradually decaying connectivity from 1 to N , 4-regular toroidal graphs, and one of the largest instance with 10,000 nodes.

D Additional Experiments

D.1 Runtime and # Params as a function of number of shots

In this section, we investigate the runtime of CTRA-PI-GNN solver as a function of the number of shots, S , compared to the runtime for S individual runs of CRA-PI-GNN solver. Fig. ?? shows each runtime as a function of the number of shots S . For this analysis, we incrementally increase the number of shots, further dividing the range of penalty parameters from 2^{-2} to 2^{17} . The results indicate that CTRA-PI-GNN solver can find penalty-diversified solutions within a runtime nearly identical to that of a single run of CRA-PI-GNN solver for shot numbers S from 2^0 to 2^{10} . However, for $S > 10^2$, we observe a linear increase in runtime as the number of shots S grows because of the limitation of memory of GPUs. Fig. 8 (right) shows the distribution of hamming distances combination,

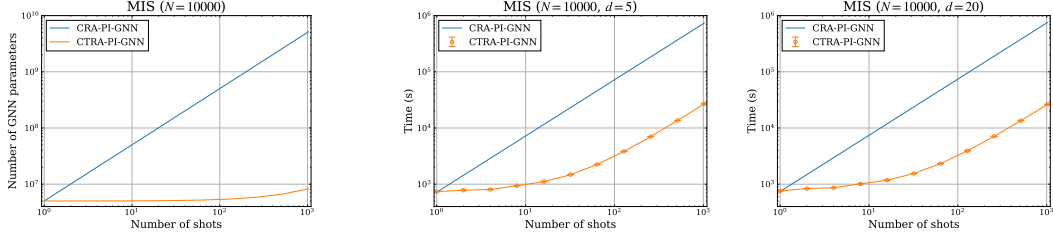


Figure 7: The runtime of the CTRA-PI-GNN solver, compared to S individual runs of the CRA-PI-GNN solver, as a function of number of shots S . Error bars represent the standard deviations of 5 random seeds.

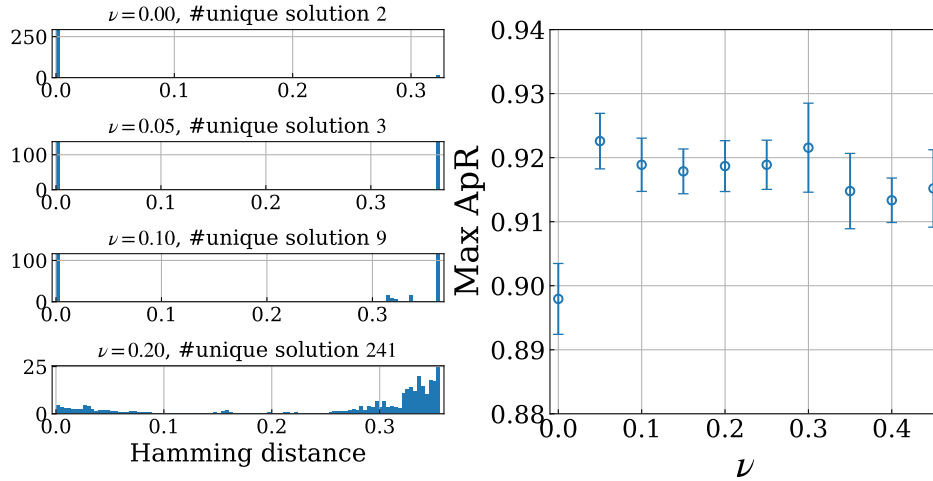


Figure 8: The density of Hamming distance combination of the solution, $\{d_H(P_{:s}, P_{:l})\}_{1 \leq s < l \leq 300}$, with different parameters ν and the count of unique solutions (left), and the maximum ApR, $\max_{s=1, \dots, 300} \text{ApR}(P_{:s})$, as a function of the parameter ν .

$\{d_H(P_{:s}, P_{:l})\}_{1 \leq s < l \leq 300}$, and the count of unique solutions with different $\nu = 0.00, 0.05, 0.10, 0.20$, whereas Fig. 7 (right) shows the maximum ApR, i.e., $\max_{s=1, \dots, 300} \text{ApR}(P_{:s})$ as a function of the parameter ν . These results indicate that the CTRA-PI-GNN solver can find more variation-diversified solutions as the parameter ν increases. Furthermore, This result indicates that the CTRA-PI-GNN solver can boost the exploration capabilities of the CRA-PI-GNN solver, leading to the discovery of better solutions.

D.2 Additional results of variation-diversified solutions for MIS

Fig. 8 (right) shows the distribution of hamming distances combination, $\{d_H(P_{:s}, P_{:l})\}_{1 \leq s < l \leq 300}$, and the count of unique solutions with different $\nu = 0.00, 0.05, 0.10, 0.20$, whereas Fig. 8 (right) shows the maximum ApR, i.e., $\max_{s=1, \dots, 300} \text{ApR}(P_{:s})$ as a function of the parameter ν . These results indicate that the CTRA-PI-GNN solver can find more variation-diversified solutions as the parameter ν increases. Furthermore, This result indicates that the CTRA-PI-GNN solver can boost the exploration capabilities of the CRA-PI-GNN solver, leading to the discovery of better solutions.

D.3 Additional results of variation-diversified solutions for MaxCut G14.

In this section, to supplement the results of the variation-diversified solutions for MaxCut G14 in Section 5.3, we present the results of the Hamming distance distribution. Fig. 9 shows the distribution of combinations of solution Hamming distances under the same settings as in Section 5.1. From these results, it is evident that the CTRA-PI-GNN solver has acquired solutions in four distinct clusters.

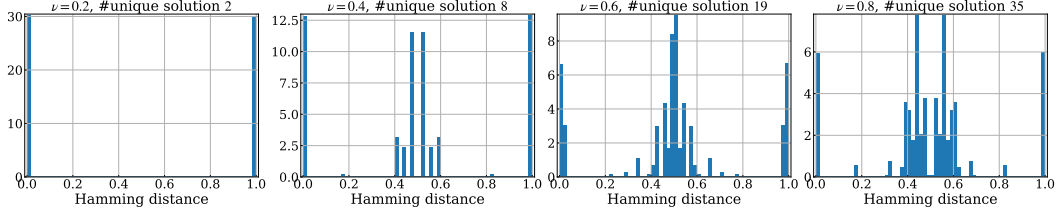


Figure 9: The density of Hamming distance combination of the solution, $\{d_H(P_{:s}, P_{:l})\}_{1 \leq s < l \leq 1000}$ in MaxCut G14, with different parameters ν and the count of unique solutions

Table 2: Numerical results for MaxCut on Gset instances

(NODES, EDGES)	CSP	PI	CRA	CTRA
G14 (800, 4,694)	0.960	0.988	0.994	0.997
G15 (800, 4,661)	0.960	0.980	0.992	0.995
G22 (2,000, 19,990)	0.975	0.987	0.998	0.999
G49 (3,000, 6,000)	1.000	0.986	1.000	1.000
G50 (3,000, 6,000)	1.000	0.990	1.000	1.000
G55 (5,000, 12,468)	0.982	0.983	0.991	0.994
G70 (10,000, 9,999)	—	0.982	0.992	0.997

D.4 Additional results for validation of exploration ability

These improvement is consistent across other Gset instances on distict graphs with varying nodes, as shown in Table. 2. In these experiment, we fix as $\nu = 6$ and evaluate the maximum ApR, $\max_{s=1, \dots, 1000} \text{ApR}(P_{:s})$. This result shows that CTRA-PI-GNN solver outperforme CRA-PI-GNN, PI-GNN, and RUN-CSP solvers.

D.5 CTRA for Multi-instance Solutions

In this section, we numerically demonstrate that the CTRA-PI-GNN solver can efficiently solve multiple problems with similar structures. The numerical experiments solve all 27 DBM instances using the CTRA-PI-GNN solver with the following loss function:

$$\hat{R}(\theta; \mathcal{C}_S, \lambda, \gamma) = \sum_{s=1}^S \hat{l}(\theta; C_s, \lambda_s) + \Phi(\theta; \mathcal{C}_S, \gamma, \alpha), \quad \Phi(\theta, \mathcal{C}_S, \gamma, \alpha) \triangleq \gamma \sum_{i=1}^N \sum_{s=1}^S (1 - (2P_{\theta, is}(C_s) - 1)^\alpha).$$

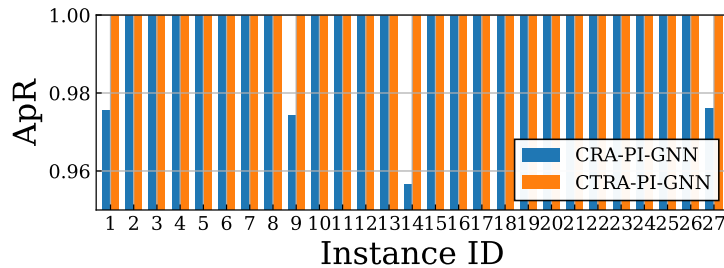


Figure 10: The ApR of DBM (Matching-1) using CTRA-PI-GNN and CRA-PI-solvers [Ichikawa, 2023].

where $C_S = \{C_s, M_s\}_{s=1}^{27}$ represents the instance parameters, and \hat{l} is defined as follows:

$$l(\mathbf{x}; C, M, \boldsymbol{\lambda}) = - \sum_{i,j} C_{ij} x_{ij} + \lambda_1 \sum_i \text{ReLU}\left(\sum_j x_{ij} - 1\right) + \lambda_2 \sum_j \text{ReLU}\left(\sum_i x_{ij} - 1\right) \\ + \lambda_3 \text{ReLU}\left(p \sum_{ij} x_{ij} - \sum_{ij} M_{ij} x_{ij}\right) + \lambda_4 \text{ReLU}\left(q \sum_{ij} x_{ij} - \sum_{ij} (1 - M_{ij}) x_{ij}\right),$$

where $\boldsymbol{\lambda}$ is fixed as $\boldsymbol{\lambda} = (\lambda_1, \lambda_2, \lambda_3, \lambda_4) = (2, 2, 12, 12)$. The parameters for the CTRA-PI-GNN solver is set the same as in Section 5.1. On the other hand, the CRA-PI-GNN solver repeatedly solve the 27 problems using the same settings as Ichikawa [2023]. As a result, the CTRA-PI-GNN solver can explore global optimal solutions for all problems. Fig. 10 showcases the solutions yielded by both the CRA-PI-GNN and CTRA-PI-GNN solvers for the 27 Matching-1 instances. Matching-2 is excluded from this comparison, given that both solvers achieved global solutions for these instances. The CRA-PI-GNN solver, applied 27 times for Matching-1, accumulated a total runtime of $36,925 \pm 445$ seconds, significantly longer than the CTRA-PI-GNN’s efficient $5,617 \pm 20$ seconds. For Matching-2, the CRA-PI-GNN solver required $36,816 \pm 149$ seconds, whereas the CTRA-PI-GNN solver completed its tasks in just $2,907 \pm 19$ seconds. The reported errors correspond to the standard deviation from five random seeds. These findings not only highlight the CTRA-PI-GNN solver’s superior efficiency in solving a multitude of problems but also its ability to achieve higher Acceptance Probability Ratios (ApR) compared to the CRA-PI-GNN solver. The consistency of these advantages across different problem types warrants further investigation.

D.6 Additional Results of penalty-diversified solutions for DBM problems

This section extends our discussion on penalty-diversified solutions for DBM problems, as introduced in Section 5.2. In these numerical experiments, we used the same Λ_S as in Section 5.2 and executed the CTRA-PI-GNN under the same settings as in Section 5.1. As shown in Fig. 11, the CTRA-PI-GNN can acquire penalty-diversified solutions for all instances of the DBM.

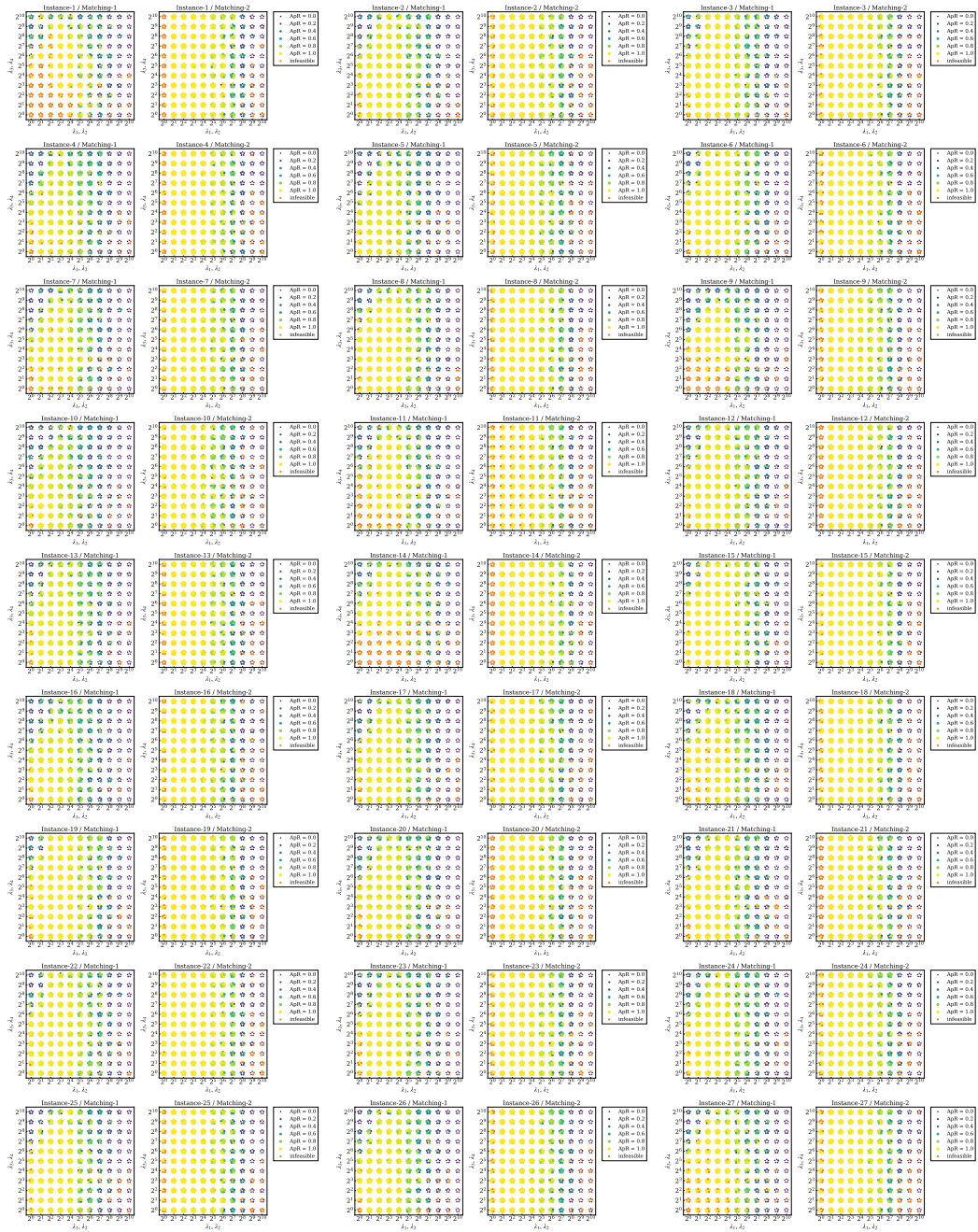


Figure 11: ApR of the DBM problems on th grid Λ_S using CTRA-PI-GNN solver. Each point on the coordinate plane represents the results from five different random seed, with the colors indicating the ApR. The constraints violation are marked with a cross symbol.